Visualization of tumor-influenced 3D lung dynamics

Anand P Santhanam[a], Cali M Fidopiastis[b], Katja Langen[c], Sanford Meeks[c], Patrick Kupelian[c], Larry Davis[d], Jannick P Rolland[a,b,e]

[a]School of Computer Science, University of Central Florida
[b]Institute of Simulation and Training, University of Central Florida
[c]Department of Radiation Oncology, MD Anderson Cancer Center
[d]Tirrion Technologies
[e]CREOL, College of Optics and Photonics, University of Central Florida

ABSTRACT

A framework for real-time visualization of a tumor-influenced lung dynamics is presented in this paper. This framework potentially allows clinical technicians to visualize in 3D the morphological changes of lungs under different breathing conditions. Consequently, this technique may provide a sensitive and accurate assessment tool for pre-operative and intra-operative clinical guidance. The proposed simulation method extends work previously developed for modeling and visualizing normal 3D lung dynamics. The model accounts for the changes in the regional lung functionality and the global motor response due to the presence of a tumor. For real-time deformation purposes, we use a Green's function (GF), a physically based approach that allows real-time multi-resolution modeling of the lung deformations. This function also allows an analytical estimation of the GF's deformation parameters from the 4D lung datasets at different level-of-details of the lung model. Once estimated, the subject-specific GF facilitates the simulation of tumor-influenced lung deformations subjected to any breathing condition modeled by a parametric Pressure-Volume (PV) relation.
Keywords: Organ Morphology, Green's Function, 3D Medical Simulation

1. INTRODUCTION

Medical simulation is a critical component to understanding and planning procedural interventions and predicting patient outcomes. Current physically based simulation techniques, such as Finite Element Modeling (FEM) and Finite Difference Modeling (FDM), extend the utility of simulating the complex anatomy and physiology into both 3D space and the fourth dimension of time.[1] Medical visualization is a critical component to planning procedural interventions and predicting patient outcomes.[2] Recent advances in computer technology provide a further revolution in medical visualization, that of coupling medical simulations with patient-specific anatomical models and their physically and physiologically realistic organ morphology.[3] An important application of such a coupling of simulation and visualization is for the treatment procedures for lung tumors, a pathophysiological lung state that is the leading cause of cancer related mortality in the United States and accounts for 29% of cancer related mortality in 2005.[4] Radiation oncology procedures aim at exposing the lung tumor of a human patient to radiation that destroys the tumor. The importance of organ movement and tracking for the radiation oncology has been previously discussed by [5, 6]. The effectiveness of the radiation oncology procedure can be significantly increased when the movement of the tumor and the overall lung can be predicted in real-time. The real-time simulation capability and the physical accuracy of the proposed deformation would facilitate the development of a real-time clinical guidance system for radiation oncology.
The main focus of our research is to simulate a patient's normal and patho-physical breathing behavior, which can then be visualized dynamically and in real-time. The end result of such an effort will provide visualization for clinicians to more accurately track and treat tumor areas as they change over time. The focus of this paper is on simulating and visualizing the patient-specific tumor-influenced lung dynamics. The method presented allows us to visualize tumor-influenced 3D lung dynamics by first estimating the deformation parameters from patient-specific high-resolution 3D lung models and then re-simulating the 3D lung dynamics under different breathing conditions modeled by the PV relation.

Medical Imaging 2006: Visualization, Image-Guided Procedures, and Display,
edited by Kevin R. Cleary, Robert L. Galloway, Jr., Proc. of SPIE Vol. 6141, 61410C, (2006)
1605-7422/06/$15 · doi: 10.1117/12.654099

The paper is further sub-divided as follows: Section 2 discusses the formation of lung tumor cells and the related work in mathematical modeling of 3D lung deformations. Section 3 briefly discusses the method adopted for modeling tumor-influenced 3D lung deformations. It is followed by a discussion on the inverse dynamics method applied for the estimation of the deformation kernel. Section 4 discusses the results and the future work of the inverse dynamics and the simulated PV curves.

2. RELATED WORKS

In this section we discuss the literature review on clinical analysis of tumor-influenced lungs and modeling lung dynamics

2.1 Lung Tumors

Healthy lungs inhale 10000 liters of air per day and during exercise they enable 2.5 liters of oxygen per minute to be exchanged through the blood-gas interface. This level of activity requires a finely tuned system of airways to direct the gas to the respiratory membranes. Unlike other body surfaces, such as skin, the non-abrasive nature of the inhaled medium does not ordinarily result in a need for a high rate of continuous cell replication. The filtration of damaging particles en route by the nasal and upper respiratory tract epithelia may not be complete especially when small particles such as carcinogenic fibers and chemicals are inhaled. Damage resulting from such particles results in cells death. The epitheleal cells of the lung possesses mechanism that can replace these dead cells. Extensive research work has been undergone in stimulating these epithelial cells for cell replication.

A brief account of these replicative cells (also known as stem cells) are as follows: The three types of replicative cells are (1) the basal cells of the bronchi, (2) the clara cells of the bronchiole and (3) type II pneumocyte of the alveoli. Of particular importance is the epithelium of the alveoli. They are mainly populated by the type I and II pneumocytes. The former constitute 86% of the alveolar surface area by virtue of their shape and mainly contributes to the gas exchange. The latter, which are secretory cells, occupies the corners of the alveoli and mainly contributes to the alveolar morphology.

Lung damage to these replicative cells can be classified into two origins: (1) mineral particles, and (2) chemical compounds. Mineral particles reach different levels of the lung based on their size and shape. Dust particles are filtered by the conducting airways and removed by mucociliary action. In contrast, roughly spherical particles that are below 5 micrometers in diameter can penetrate the alveoli and may become lodged there with much potential for long-term damage. Most of these cells are indigestible and result in the death of the cells and the formation of fibrosis. More importantly, dusts reaching the type II pneumocytes may promote the release of excess amounts of surfactant which can fill the alveoli. Type I cells are exquisitely sensitive to these dust particles. It was also shown in an animal study that these particles since their exposure to the animals were retained by the animals in their lungs for over a year. Thus the presence of these dust particles in the alveoli leads to cell death of type I pneumocytes and the cell replication process is initiated by the type II pneumocytes. Chemical compounds such as nitrogen dioxide or the supra normal oxygen affect the alveolar epithelium which subsequently leads to the death of type I pneumocytes. Upon return to normal conditions the epithelium recovers during which the type II cells rise dramatically without a concomitant rise in the type I cells. Thus the gas exchange process of the alveoli is significantly reduced. Based on the level of exposure to these chemical compounds the damage to type I pneumocytes occur. Additionally the presence of high levels of type II pneumocytes in the alveolar epithelium leads to the creation of cell tumors.

2.2. Lung Deformations

Lung deformations have been studied for verifying different brands of medical imaging equipments such as myocardial SPECT, [7-9] understanding pulmonary mechanics, [10-12] registering MRI images,[13] [14] generating in-vitro lung models,[15] and for medical training purposes [16]. The initial methods developed to model 3D human lung deformations were based on physiology and clinical measurements.[17] Significant amount of work has been undergone in understanding and modeling pulmonary mechanics using animal and human data. Key parameters extracted from pulmonary imaging modalities are the Green's strain tensor and Jacobian of the displacement gradient. While the Lagrangian strain tensor quantifies the change in length of the edges in the 3D data, the Jacobian of the displacement gradient provides information regarding the local change in lung volume.

From a simulation and visualization perspective, we concentrate on deforming a given 3D human lung model for a known air-flow entering the lungs. It is accomplished using both the stress and strain components at every lung node and using a physics-based deformation paradigm that relates the stress and strain in a local lung neighborhood. Under this context, the human lung modeling literature has been mainly divided into two approaches: (1) Single compartment model and (2) multi-compartment model. The physically-based deformation of the human lung model as a linearized single-compartment model was proposed by Promayon.[18] An FEM based single-compartment model was proposed by Decarlo for real-time medical visualization.[19] It was then extended by Kaye in order to model pneumothorax related conditions.[20] Additionally, a visualization-based training method was developed for pneumothorax using a single-compartment model.[16] The method had an analogy for lung deformations to an electrical circuit.[20] A multi-compartment functional FEM model, which modeled the tissue constituents (i.e. parenchyma, bronchiole and alveoli) of lungs was done by Tawhai. This effort aimed in analyzing the anatomical functions of lungs during breathing.[21] The run-time computational complexity of this approach was reduced by modeling solely the bronchioles and the air-flow inside the lung.[22] Of particular importance is the role of air-flow inside lungs. Based on medical image analysis, the spatial air distribution inside lungs was shown to be dependent on the gravity and thus the orientation of the subject. From the perspective of a physically-based deformation, the air distribution defines the force applied on the lung model and thus needs to be accounted for./

A non-physically based analysis of lung morphology has been extensively investigated in the field of lung physiology and imaging. Some of the key works include the analysis of lung morphology using image warping.[23] A non-physically-based method to lung deformations was also proposed using NURBS surfaces based on imaging data from CT scans of actual patients.[8] The usage of a high-resolution model for lung deformations and its real-time visualization were not addressed in these efforts. From a modeling and simulation perspective, the physically-based deformation methods are apt for simulating lung dynamics since they allow the inclusion of different breathing parameters.

3. METHODS

The method adopted for modeling tumor-influenced lung dynamics takes into account both the behavioral and anatomical changes in the thoracic system. The behavioral changes take into account the summary muscle resistance caused by the diaphragm and rib-cage and is as discussed in [24-26]. The anatomical changes are taken into account by first estimating the elastic properties of tumor-influenced 3D lung models which allows a physically-based method to model the tumor-influenced lung deformations. The estimated deformation operator encapsulates the effects of tumor discussed in section 2.1. The approach adopted for such estimation is to first use a forward lung dynamics that can account for the morphological changes from one 3D model to another during breathing. The forward lung dynamics is further discussed in section 3.1. The method to estimate the deformation operator and model the changes in the PV relation are discussed in section 3.2 and 3.3 respectively.

3.1 Forward lung dynamics

In this section we outline the methodology adopted for the dynamic simulation of 3D lungs deformation. This method is sub-divided into two components, which has been addressed in [25, 27] and [28]. In the first component we parameterized the change in lung volume for a change in pressure referred to as trans-pulmonary pressure. This change in pressure, which causes the air-flow inside lungs, accounts for both the local muscle resistance caused by anatomical components, such as lung tissue, diaphragm and rib-cages, as well as the motor drive of breathing controlled by a network of neurons in the medulla. The relation between the lung volume and the trans-pulmonary pressure is referred to as a PV relation. Both normal and abnormal PV relations may be simulated.

In the second component we estimated the change in the global lung shape for an increase in lung volume[28]. This was obtained using a physically-based deformation method. For real-time purposes, a single compartment based approach are used for modeling the lung deformations. Within the context of computer animation, a GF-based deformation was chosen since it facilitates multi-resolution representation of lung models (extending from macroscopic to microscopic levels). In the implementation discussed in this paper the total number of nodes on each of the 3D high-resolution lung models is approximately 400,000.

From a physically based approach, a Young's modulus (YM) was first associated to every node of the 3D lung model based on the lung's regional alveolar expansion. A unit force was then applied on each node and a transfer function

matrix was computed using an iterative approach. In each step of the iteration, the force applied on a node was shared with its neighboring nodes based on a local average of YM as described in [28]. The iteration stopped when the sharing of applied force reached equilibrium. At this point of equilibrium the force shared by a node with its neighbors formed a row of the transfer function matrix. An upright orientation was considered in order to deform the 3D lung model. The applied force due to the air-flow inside the lungs was given by the vertical pressure gradient of lungs[23, 29, 30]. The computed force was then normalized so that the sum of the applied force magnitude on all the nodes was equal to a unit increase in volume. A unit increase in volume was set as the ratio between the tidal volume of human lungs (i.e. 500 ml) and the product of the deformation steps per second (i.e. 66.66 steps/sec) by the ventilation rate of inhalation or exhalation (normally 5 sec/breathing). Thus for each increase in lung volume the subsequent change in lung shape was computed[28].

A GPU-based computational optimization of the 3D lung dynamics was described in [31]. We considered a per-vertex approach for deforming and rendering 3D lung models. We presented a method to optimally compute the matrix-vector multiplication in a GPU during run-time. Specifically the matrix-vector multiplication was represented in steps, which can be partially pre-computed off-line. The columns of the transfer function matrix were pre-computed and represented using SH coefficients. These coefficients were obtained from orthonormal decomposition of the transfer function matrix using SH transformations[32]. The per-vertex nature of SH coefficients allowed us to use GPU for improving the computation-speed.

3.2 Estimation of deformation parameters for tumor-influenced 3D lung deformations

In this section we present a method to estimate the deformation operator, which represents the inter-nodal elastic interaction. The estimated kernel can then be used for deforming lung models at any physical condition as previously shown in [31]. Additionally, the YM of every node can also be estimated from the deformation kernel allowing us to simulate variations in elasticity.[28, 33]

We take as input two 3D CT datsets (one at the start and another at the end of the inhalation) obtained using breath-hold procedure and a theoretical estimation of the airflow during the imaging process. We then extract 3D polygonal models from each of the 3D-CT datasets. As a reference, we also consider another 4D CT dataset of a normal human subject previously used in [33]. We shall now discuss in Section 3.2.1 the steps for computing the nodal displacements. We shall then discuss the relation derived for estimating the transfer function in 3.2.2.

3.2.1 Preliminary data processing

The direction and the magnitude of the displacement vector associated with each node is now computed as follows. We employ the method discussed in [33] to obtain the directions of the model's nodal displacement. Let ***min*** and ***max*** be two vectors that represent the bounding co-ordinates of the lungs at the start of inhalation. Let $\boldsymbol{p}_i$ be the position of node i at the start of inhalation, and $\boldsymbol{d}_i$ be a vector that represents the displacement direction of node i. Under the hypothesis that the direction of displacement is constant, the components of $\boldsymbol{d}_i$ may be simply modeled as first-order polynomials given by

$$d_i.X = c_1 \times \left(\frac{p_i.X - \min.X}{\max.X - \min.X} \right)^{c_2}, \tag{1}$$

$$d_i.Y = c_3 \times \left(\frac{p_i.Y - \min.Y}{\max.Y - \min.Y} \right)^{c_4}, \tag{2}$$

$$d_i.Z = c_5 \times \left(\frac{p_i.Z - \min.Z}{\max.Z - \min.Z} \right)^{c_6}, \tag{3}$$

where c_1, c_2, c_3,c_4, c_5, and c_6 are direction constants. Based on our previous analysis, the values of the constants are set as shown in Table.1. In order to compute the magnitude of the nodal displacement, a ray from each node of the 3D model at the start of inhalation is projected to intersect with the 3D model at the end of the inhalation. The magnitude of the projected ray of each node is considered as the required magnitude of the nodal displacement.

Table.1 Tabulation of direction constants

Lung	C1	C2	C3	C4	C5	C6	C7	C8	C9
Left	0.09	0.23	0.4	0.5	0.1	2.3	0.01	0.95	0.07
Right	0.09	0.22	0.39	0.51	0.11	2.2	0.01	0.96	0.05

3.2.2 Deformation Operator.

The general formula of the GF as an operator in continuous space is given as

$$D(I) = \sum_J K(J,I) \times f(J), \tag{4}$$

where *D(I)* is the displacement of the node *I*, *f(J)* is the force applied on node *J,* and *K(J,I)* is the GF operator (deformation kernel), which represents the elastic interaction between nodes taking into account both the inter-nodal distance and elastic properties. The general form of the kernel row is described in two different representations. The first one is given as

$$K(J,I) = P_I \cos z(J,I) + Q_I \sin z(J,I), \tag{5}$$

where $z(J,I)$ is a function that returns a value in the range of zero to 2π .[34] P_I and Q_I are arbitrary constants that take values between zero to 1.[35] Such a representation of the kernel row is also referred to as a discrete spectral representation. The values of P_I and Q_I can be arbitrarily varied in order to simulate variations in the breathing conditions. With respect to the lung dynamics, the steerable constants of the discrete spectral representation can be used to model variations induced by diaphragm and abdominal movements. The above equation represents the kernel as a continuous trigonometric function discretized by the values of $z(J,I)$. A further mathematical simplification of equation (5) can be given as

$$K(J,I) = C_I \cos z'(J,I), \tag{6}$$

where C_I is an arbitrary constant and $z'(J,I)$ is a function that returns a value in the range of 0 to $\pi/2$. Equation (6) represents a row of the kernel matrix as a cosine function. The second general form of the kernel row is described as a proportionality function of the piecewise Euclidean distance *d(J,I)* between *I* and *J*.[36] It can thus be written as

$$K(J,I) = \frac{D_I}{4\pi d(J,I)}, \tag{7}$$

where D_I is a proportionality constant, which depends on the deformation mechanics of the lungs. Equation (7) has been used for modeling unique cases pertaining to the mechanics. These unique cases discussed by Stakgold presents the different values of the proportionality constant.[35] In the case of lungs, the proportionality constant D_I remains unknown. We now merge the two definitions of the kernel in order to solve for *z'(J,I)*. Since both C_I and D_I of equation (6) and (7) act as proportionality constants, the values of cos(z'(J,I)) and $\frac{1}{4\pi d(J,I)}$ can be equated. *z'(J,I)* can now be written as

$$z'(J,I) = \left[\cos^{-1}\left(\frac{1}{4\pi d(J,I)}\right) \right]. \tag{8}$$

It can be seen that for higher values of the Euclidean distance between *J* and *I*, the value of *K(J,I)* tends to zero. Additionally, the values of *z'(J,I)* and *d(J,I)* are proportional. However, in the case of lungs we consider a heterogenous elastic representation in order to account for the regional variations in the alveolar expansion. Thus equation (8) is modified as

$$z'(J,I) = \left[\cos^{-1}\left(\frac{1}{4\pi d'(J,I)}\right) \right] \quad , \tag{9}$$

where *d'(J,I)* is a function that takes into account both the distance and the local elastic properties. For higher values of *d'(J,I)* the value of *K(J,I)* tends to zero. An initial representation for *d'(J,I)* is given as a linear combination of the distance and the elastic interaction.

$$d'(J,I) = A_I d(J,I) + B_J e(J,I), \tag{10}$$

where A_I and B_I are arbitrary constants. These constants are also referred to as structural constants in the paper, since they both compute the function *d'*. The function *e(J,I),* which represents the elastic interaction between nodes *J* and *I,* is given as a difference in the alveolar expansion of the region surrounding nodes *J* and *I*. Such a representation is based on the fact that the air flows to the region of least resistance, which in our case is the region of higher alveolar expandability. The regional alveolar expandability is thus an indirect indicator of the YM. The regional alveolar expandability has been previously discussed in [37], [38], and [29]. The function *e* is thus defined as

$$e(J,I) = a(J) - a(I), \tag{11}$$

where *a(J)* is a function representing an estimated alveolar expandability in the region surrounding node *J*. The definition of the function in terms of the alveolar expansion is an essential factor in estimating the kernel for the 3D lungs. It can be seen that the inverse lung deformation problem mathematically relates to computing the values of A_I, B_I, and C_I for each node *I*. We now continue our discussion on (i) estimating the values of A_I ,B_I, and C_I for each node *I*, and (ii) estimating the values of P_I , Q_I and the function *Z'(J,I)*.

A method to estimate the values of A_I and B_I using simultaneous equation based representation of equation (9) coupled with approximated kernels, discussed in [33], is as follows. For the 3D lung model extracted from the patient-data, two different estimates of the deformation kernel are first computed. Each deformation kernel is estimated, using only the structural parameters (piecewise Euclidean distance, and regional alveolar expandability). The second kernel is computed with the distance between any two nodes to be twice as that of the distance used in the estimation of the first kernel. Now using equation (7) we form two simultaneous equations for each node I, with the unknown being A_I and B_I. One may also note that D_I is eliminated in these equations. The values for the structural constants for each node are thus solved. The value of C_I can be computed using equation (5) as

$$C_I = \frac{D[I]}{\sum_{J=0}^{N} f[J] \times \cos(z'(J,I))}. \tag{10}$$

The values of C_I for left and right lung models are plotted in Fig 1a and 1b respectively. For comparison purposes, we show the values of C_I for normal left and right lung models in Fig 1c and 1d. It can be seen that changes in both the left and right lungs can be seen in tumor-influenced lung dynamics when compared to normal lungs. Such changes are attributed to the effects caused by the tumor.

Now the values of P_I and Q_I can be written as

$$P_I = C_I \cos\phi_I \text{ and } Q_I = C_I \sin\phi_I, \tag{11}$$

where ϕ_I is an arbitrary parameter that takes value between *0* to 2π . The variations in lung deformations induced by varying the values of ϕ_I are discussed in section 4.

3.3 Pressure-Volume relation

Changes in the PV curve are caused by the additional work during inspiration and expiration,[39] and are modeled using a bio-mathematical model discussed in [40]. The PV relation during inhalation and exhalation is represented using a second-order differential equation with a variable parameter. This parameter is further computed as a linear summation of products of a set of control parameters and trigonometric basis functions that represent the summary muscle resistance. The values of control parameters are extracted from patient's specific clinical data.[41] We simulate a PV curve that represents tumor-influenced lung dynamics by varying the normal control constants discussed in [41]. One key property of the control constants that we use is that they form a converging sequence and the rate of convergence is observed to be slower under lower drive conditions. We thus decrease the rate of convergence of control parameters during inhalation by first multiplying every parameter with its exponent and then dividing the resultant with the exponent of the first parameter in order to keep the parameters in the same range of values. Let C_i^{inh} and C_i^{exh} be the

array of control constants during inhalation and exhalation and let d_i^{inh} and d_i^{exh} be the modified control constants respectively. The method to vary the control constants is given by

$$d_i^{inh} = C_0^{inh} \times \frac{\log\left(C_i^{inh} \times \varphi\right)}{\log\left(C_0^{inh} \times \varphi\right)} \quad , \tag{12}$$

$$d_i^{exh} = C_0^{exh} \times \frac{\log\left(C_i^{exh} \times \varphi\right)}{\log\left(C_0^{exh} \times \varphi\right)} \quad , \tag{13}$$

where φ is a proportionality constant that relates the change in control constants to the amount of additional work. For experimental analysis the value of φ is set to 0.1. The PV curve generated for the modified control constants is shown in Fig 2.

4. DISCUSSION

Through our research we aim to extend the thoracic simulation paradigm to include real-time visualization of both normal and pathophysical 3D lung dynamics. This is achieved by estimating the deformation operator from a given patient data (discussed in section 3.2.2) and simulating the lung dynamics using a GPU based optimization (briefly discussed in section 3.2.1 and detailed in [31]). Such an approach coupled with the PV relation (discussed in section 3.3) allows us to simulate tumor-influenced 3D lung deformations. The usage of a physically-based deformation approach for lung deformations allows us to model lung deformations with varations in physics-based parameters. Results of the 3D lung deformations are as shown in Fig 3a and 3b. Fig 3a shows the initial shape of lungs at the start of inhalation and Fig 3b shows the shape of lungs at the end of the inhalation cycle.

The proposed framework takes into account the changes in deformation constraints imposed by the tumor (through the PV curve) on the lung's air-volume. The deformation operator is represented using the discrete spectal representation of the GF, which facilitates obtaining physically-realistic variations of 3D lung deformation caused by variations in the rib-cage and diaphragm movements. The feasibility of simulating such variations in demonstrated in Fig.4a and 4b. For example, in Fig 4a the value of ϕ_I was set to the normalized distance from the supporting surface (posterior side of lungs). In Fig 4b the the value of ϕ_I was set to the square of the normalized distance from the supporting surface. The accuracy of such variations needs to be further verified and will be discussed in future investigations.

The choice of a single compartmental model enables visualization of high-resolution 3D lung deformations. The accuracy in the usage of single compartmental model has been validated by some of the peers. The validation however needs to be performed for tumor-influenced lung dynamics across a wide range of human subjects of various age and race. The simulated lung dynamics also needs to be compared with 4D HRCT images of tumorous lung subjects with different breathing conditions. Also, the direction constants (discussed in section 3.2.1) also need to be analyzed using tumorous 4D HRCT images for its correspondence with normal 4D HRCT images.
The usage of the regional alveolar expandability (function *a*) as one of the parameters allows the proposed method to account for the physiology of human subjects. The variations in the alveolar expandability caused by a tumor need to be investigated by analyzing the CT datasets of tumor-influenced subjects across a wide range of age and race. The results of such an analysis will be discussed in future investigations. One may also note that the variations in the air constituents can lead to changes in the alveolar blood pressure, which subsequently alters the alveolar expandability. The proposed method can be expanded in order to address this aspect of the lung physiology.

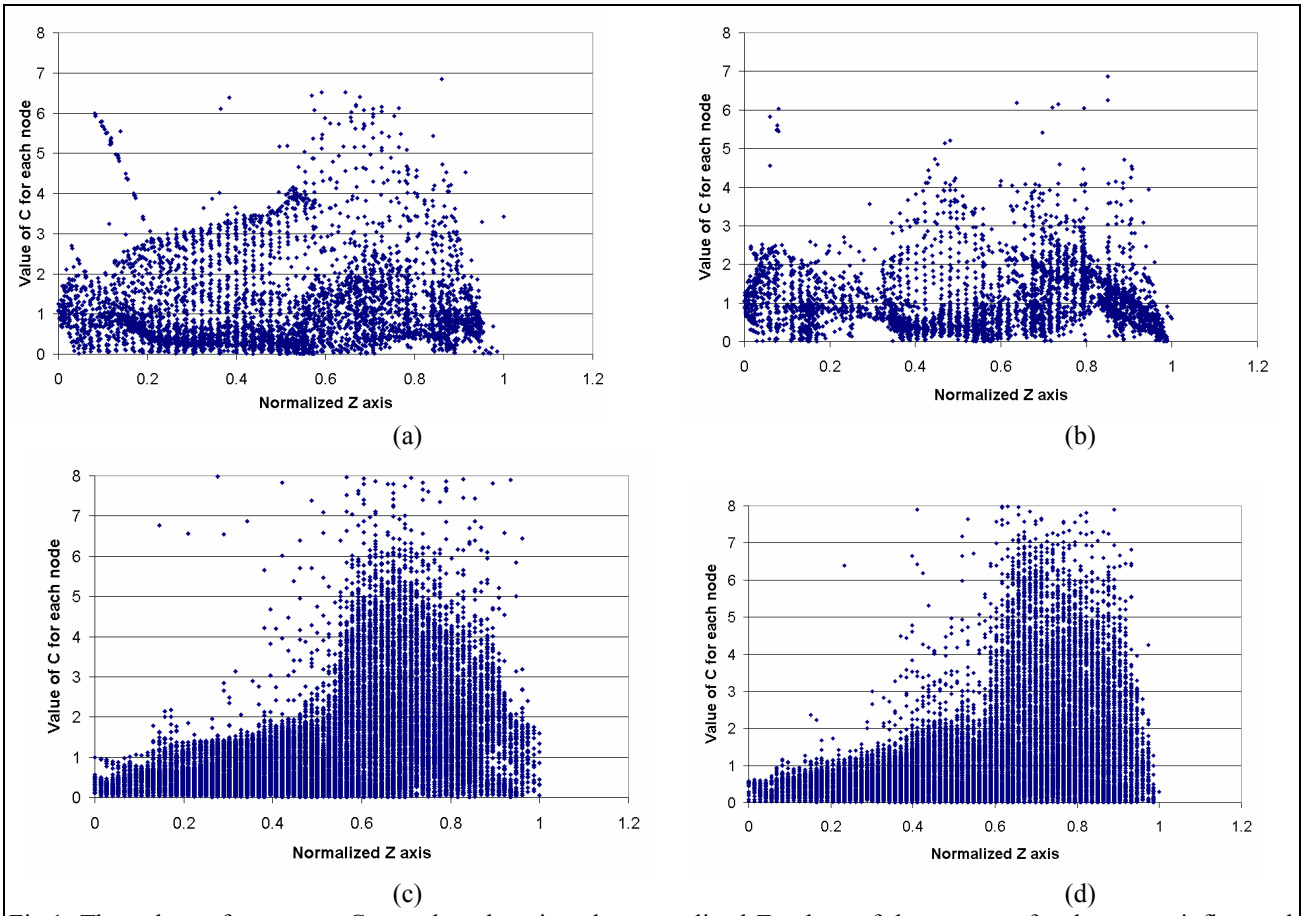

Fig.1. The values of constants C_I are plotted against the normalized Z values of the vertexes for the tumor-influenced left and right lung ((a) and (b)) and normal left and right lung ((c) and (d).

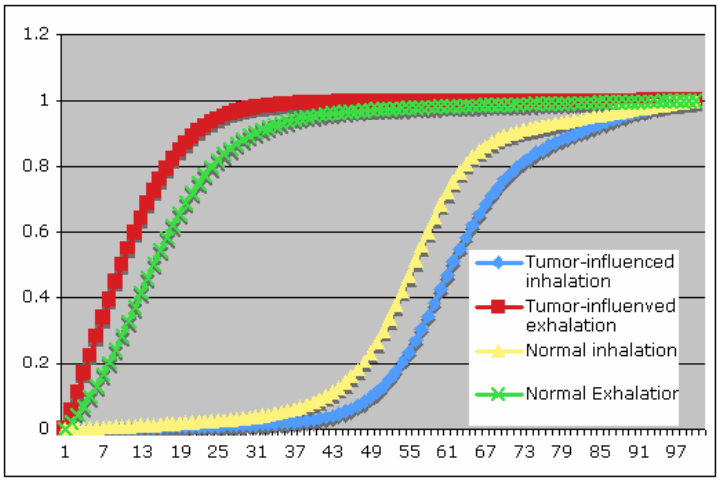

Fig 2. Normalized PV curve simulated for tumor-influenced lung dynamics.

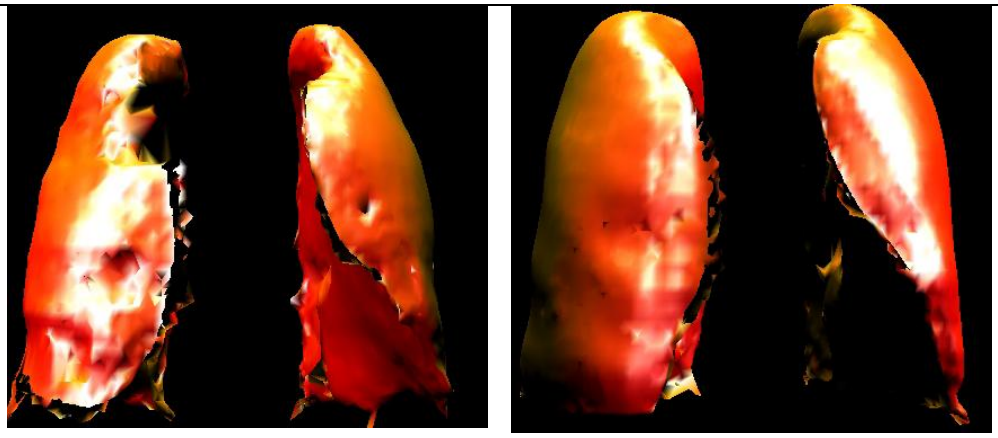

(a) (b)

Fig.3. 3D models of tumor-influenced lungs (a) at the start of inhalation and (b) at the end of inhalation.

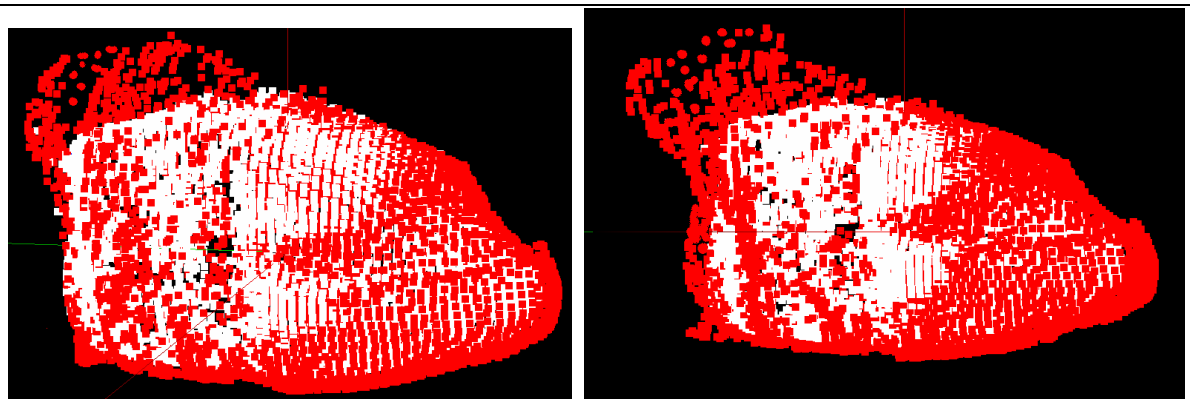

(a) **(b)**

Fig4. 3D deformed point-cloud models (red color) of tumor influenced lungs superimposed over 3D point-cloud models (white color) at the start of inhalation. Variations induced in the deformation is simulated by (a) setting the value of ϕ_I for each node *I* to the normalized distance from the supporting surface (posterior side of lungs), and (b) setting the value of ϕ_I for each node *I* to the square of the normalized distance from the supporting surface.

Acknowledgements: This work is funded by the Link foundation and the Florida Photonics Center of Excellence. We thank Dr. Mudur Pandurang (Concordia University) for his constructive comments on the algorithm.

References

1. Robb, R.A., *Three-dimensional visualization in medicine and Biology*, in *Handbook of medical Imaging: Processing and Analysis*, I.N. Bankman, Editor. 2000, Academic Press: San Diego,CA.
2. Nye, L.S., *The minds' eye.* Biochemistry and Molecular Biology Education, 2004. **32**(2): p. 123-131.
3. Good, M.I., *Patient Simulation for training basic and advanced clinical skills.* Medical Education, 2003. **37**: p. 14.
4. Epidemiology and Statistic Unit, A.L.A., *Trends in Lung Cancer Morbidity and Mortality*. 2005. p. 1-23.
5. Murphy, M.J., *Tracking moving organs in real time.* Seminars on Radiation Oncology, 2004. **14**(1): p. 91-100.
6. Shirato, H., Y. Seppenwoolde, K. Kitamura, R. Onimura, and S. Shimizu, *Intrafractional tumor motion: lung and liver.* Seminars on Radiation Oncology, 2004. **14**(1): p. 10-18.
7. Segars, W.P. and B.M.W. Tsui, *Study of the efficacy of respiratory gating in myocardial SPECT using the new 4D NCAT phantom.* IEEE Transactions on Nuclear Science, 2002. **49**(3): p. 675-679.
8. Segars, W.P., D.S. Lalush, and B.M.W. Tsui, *Modeling respiratory mechanics in the MCAT and the spline-based MCAT systems.* IEEE Transactions on Nuclear Science, 2001. **48**(1): p. 89-97.
9. Segars, W.P., *Development of a new dynamic NURBS-based cardiac-torso (NCAT) phantom*. 2002, University of North Carolina: Chapel-hill.
10. Hoffman, E.A., A.V. Clough, G.E. Christensen, C.L. Lin, G. McLennan, J.M. Reinhardt, B.A. Simon, M. Sonka, M. Tawhai, E. Van Beek, and G. Wing, *The comprehensive imaging-based analysis of the lung.* Academy of Radiology, 2004. **11**: p. 1370-1380.
11. Gee, J.C., T. Sundaram, I. Hasegawa, H. Uenatsu, and H. Hatabu. *Characterization of regional pulmonary mechanics from serial MRI data*. in *Medical Image Computing and Computer Aided Intervention*. 2002: LNCS.
12. Voorhees, A., J. An, K. Berger, R.M. Goldring, and Q. Chen, *Magnetic resonance imaging-based spirometry for regional assessment of pulmonary function.* Magnetic Resonance in Medicine, 2005. **54**: p. 1146-1154.
13. Reinhardt, J.M., R. Uppaluri, W.E. Higgins, and E.A. Hoffman, *Pulmonary imaging and analysis*, in *Handbook of medical imaging*, M. Sonka and J.M. Fitzpatrick, Editors. 2000. p. 1005-1060.

14. Sundaram, T., B.B. Avants, and J.C. Gee. *Towards a dynamic model of pulmonary parenchymal deformation: evaluation of methods for temporal re-parameterization of lung data*. in *Medical Image Computing and Computer Aided Intervention*. 2005: Lecture notes on Computer Science.
15. Guerrero, R.R., D.E. Rounds, and J. Booher, *An improved organ culture method for adult mammalian lung.* InVitro, 1977. **13**(8): p. 517-524.
16. Dawson, S., *A critical approach to medical simulation.* Bulletin of the american college of surgeons, 2002. **87**(11): p. 12-18.
17. Ligas, J.R. and F.P.J. Primiano, *Respiratory mechanics*, in *Encyclopedia of Medical Instrumentation*, J.G. Webster, Editor. 1988, John Wiley& Sons: New York. p. 2550-2573.
18. Promayon, E., P. Baconnier, and C. Puech, *Physically-based model for simulating the human trunk respiration movements.* Proceedings of International Joint Conference in CVRMED and MRCAS., 1997. **1205**: p. 121-129.
19. Decarlo, D., J. Kaye, D. Metaxas, and J.R. Clarke. *Integrating Anatomy and Physiology for behavior modeling*. in *MMVR*. 1995.
20. Kaye, J.M., F.P.J. Primiano, and D.N. Metaxas, *A Three-dimensional virtual environment for modeling mechanical cardiopulmonary interactions.* Medical Image Analysis, 1998. **2**(2): p. 169-195.
21. Tawhai, M.H. and K.S. Burrowes, *Developing integrative computational models.* Anatomical Record, 2003. **275B**: p. 207-218.
22. Ding, H., Y. Jiang, M. Furmancyzk, A. Prkewas, and J.M. Reinhardt. *Simulation of human lung respiration using 3-D CFD with Macro Air Sac System*. in *Western Simulation Conference Society for Modeling and Simulation International*. 2005. New Orleans.
23. Krishnan, S., K.C. Beck, J.M. Reinhardt, K.A. Carlson, B.A. Simon, R.K. Albert, and E.A. Hoffman, *Regional lung ventilation from volumetric CT scans using image warping functions.* 2004.
24. Santhanam, A., C. Fidopiastis, and J.P. Rolland. *A Biomathematical model for pre-operative visualization of COPD and Associated Dyspnea*. in *NIH Symposium on Biocomputation and Bioinformation*. 2003. Washington.D.C.
25. Santhanam, A., C. Fidopiastis, and J.P. Rolland. *An adaptive driver and real-time deformation algorithm for visualization of high-density lung models*. in *Medical Meets Virtual Reality 12*. 2004. Newport, CA: IOS Press.
26. Santhanam, A., C. Fidopiastis, J.P. Rolland, and P. Davenport, *A bio-mathematical formulation for modeling the pressure-volume relationship of lungs (Submitted).* IEEE Transactions on Information Technology and Biomedicine, 2005.
27. Santhanam, A., C. Fidopiastis, J.P. Rolland, and P. Davenport, *A bio-mathematical formulation for modeling the pressure-volume relationship of lungs (submitted).* Journal of Applied Physiology, 2004.
28. Santhanam, A., C. Fidopiastis, F. Hamza-Lup, J.P. Rolland, and C. Imielinska. *Physically-based deformation of high-resolution 3D lung models for augmented Reality based medical visualization*. in *Medical Image Computing and Computer Aided Intervention, AMI-ARCS*. 2004. Rennes,St-Malo: Lecture Notes on Computer Science.
29. West, J.B., *Respiratory physiology, the essentials*. 1995, Philadelphia,USA: Lippincott Williams and Wilkins.
30. Fan, L., C.-W. Chen, E.A. Hoffman, and J.M. Reinhardt. *Evaluation and application of 3D lung warping and registration model using HRCT images*. in *Proc. SPIE Conf. Medical Imaging*. 2001. San Diego,CA.
31. Santhanam, A. and J.P. Rolland, *3D lung dynamics using a programmable graphics hardware (submitted).* IEEE Transactions on Information Technology and Biomedicine, 2005.
32. MacRobert and T. Murray, *Spherical harmonics an elementary treatise on harmonic functions with applications*. International series of monographs in pure and applied mathematics. 1967, New York: Oxford Pergamon Press.
33. Santhanam, A., C. Imielinska, P. Davenport, and J.P. Rolland, *Modeling and simulation of Real-time 3D lung dynamics(submitted).* IEEE Transactions on Information Technology and Biomedicine, 2005.
34. Zeidler, *Applied functional analysis: applications to mathematical physics*. Applied mathematical sciences, ed. J.E. Marsden. 1998.
35. Stakgold, I., *Green's functions and boundary value problems*. Mathematical physics. 1979: Wiley Interscience.
36. Griffel, D.H., *Applied functional analysis*. 2002, New York,NY: Dover Publications.
37. Calverley, P.M.A., *Chronic Obstructuve Pulmonary Disease*, ed. P.M.A. Calverley and N. Pride. 1995, London: Chapman and Hall Medical.

38. Jardins, T.D., *Cardiopulmonary anatomy and physiology*. Essentials of Respiratory care. 1998, Champaign,Illinois: Delmar Publishers.
39. Visaria, R. and D. Westenkow. *Diagnosis of pulmonary complications based on Airway Pressure-Flow waveforms*. in *Proceedings of the Second Joint EMBS/BMES Conference*. 2002. Houston,TX: IEEE.
40. Santhanam, A., C. Fidopiastis, and J.P. Rolland, *An adaptive driver and real-time deformation algorithm for visualization of high-density lung models.* MMVR, 2004. **98**: p. 333-339.
41. Takeuchi, M., K.A. Sedeek, P. Guilherme, P. Schettino, K. Suchodolski, and R.M. Kacmarek, *Peek Pressure During Volume History and Pressure-Volume Curve Measurement affects Analysis.* American Journal of Respiratory Critical Care, 2001. **164**: p. 1225-1230.